Available online at www.sciencedirect.com
SCIENCE DIRECT®
Composites Science and Technology 65 (2005) 1869–1879
COMPOSITES SCIENCE AND TECHNOLOGY
www.elsevier.com/locate/compscitech

Progress in the fabrication of ultra-high-temperature ceramics: "in situ" synthesis, microstructure and properties of a reactive hot-pressed HfB_2–SiC composite

Frédéric Monteverde *

National Research Council, Institute of Science and Technology for Ceramics, Via Granarolo 64, 48018 Faenza, Italy

Received 4 October 2004; received in revised form 23 March 2005; accepted 9 April 2005
Available online 12 May 2005

Abstract

An ultra-high-temperature HfB_2–SiC composite was successfully fabricated by reactive hot-pressing. Solid reagents like Hf/Si/B_4C, mechanically mixed in molar ratio 2.2/0.8/1, were "in situ" converted into the basic ingredients (i.e., HfB_2, SiC), and then directly hot-pressed until full density was achieved (1900 °C final temperature). The microstructure consisted of faceted diboride grains (mean size 3 μm), with HfC (6 vol%) and SiC (22 vol% and mean size 1 μm) evenly distributed intergranularly. The combination of some mechanical properties was of considerable significance: about 19 GPa of micro-hardness, 520 GPa of Young's modulus, 770 ± 35 and 315 ± 10 MPa of flexural strength at 25 and 1500 °C, respectively. A relevant merit characterized the resistance to oxidation: repeated exposures at 1700 °C, or at 1450 °C for 20 h, involved limited mass gains and small changes of the original microstructure. The marked refractoriness of HfB_2 and SiC, which constitute the framework of the composite, dominates beneficially its thermostructural stability.

Keywords: Ultra-high temperature ceramic (UHTCs); Microstructure; Thermomechanical properties; Oxidation; Reactive hot-pressing

1. Introduction

The design and processing of materials with enhanced high temperature capabilities represent one of the most challenging task of modern engineering. Within the crowded families of advanced engineered ceramics, transition metal diborides and carbides are naturally selected for ultra-high-temperature structural applications (for instance furnace elements, crucibles, arc-plasma electrodes, thermal protection) because of melting points exceeding 3000 °C, coupled to an overall thermostructural stability at very high temperatures [1]. Great attention is currently addressed towards the engineering of ultra-high-temperature ceramics (UHTCs) capable to increase the toleration of heat on sharp leading profiles of space vehicles reentering the Earth's atmosphere [2–5].

During recent decades, a core of attention of the scientific community has been focused on the design of ceramic matrix composites (CMCs), owing to the shared opinion among researchers that the development of monolithic ceramics may secure only marginal performance benefits. CMCs have been largely produced by densification of mechanically mixed powders. Since the melting points of the UHTCs are among the highest known, processing them into CMCs with final complex shapes and full density requires long exposure in atmosphere-controlled conventional furnaces at extremely high sintering temperatures and applied pressures.

As an alternative route, CMCs have been proved being manufactured using "in situ" high-temperature

* Tel.: +390546699758; fax: +39054646381.
E-mail address: fmonte@istec.cnr.it.

0266-3538/$ - see front matter © 2005 Elsevier Ltd. All rights reserved.
doi:10.1016/j.compscitech.2005.04.003

solid-state chemical displacement reactions [6–8]. The advantage of this approach is that it has offered the possibility to obtain composites not only with controlled microstructure, but also characterized by an high chemical compatibility of the "in situ" formed individual phases evenly distributed. With the ability to adjust the final microstructure being understood, the proposal of unexplored routes is additionally motivated by the demand for reducing manufacturing costs (for instance, cheaper raw powders and processing steps). Unlike self-propagating high-temperature synthesis (SHS), that basically exploits the exothermicity of uncontrolled chemical reactions, a displacement reaction synthesis can be accomplished gradually via solid-state diffusion at temperatures below that ignited once a (triggered) SHS takes place [9]. It ensures better control over the final microstructure and the isotropy of properties.

Superior UHTCs would be a great asset to improving the capabilities of spacecrafts. Current research into thermal insulating structures is aimed at designing innovative UHTCs for sharp leading edges of hypersonic space vehicles. These new materials should combine the potentiality to withstand extremely high temperatures to the capacity of dissipating heat efficiently [1,3]. The poor sinterability and the resistance to oxidation/ablation, which represent topical deficiencies in the UHTC class of materials, are addressed with an appropriate focus on compositional designs and composite constructions [3,10,11].

Following what has been just reported, the present paper intended to produce by reactive hot-pressing an HfB_2–SiC composite which (to date) does not draw on already published data. "In situ" synthesis and sintering, microstructure and some thermostructural properties were studied and discussed.

2. Experimental

Three commercial solid precursors like Hf (99.8% pure, FSSS 2.1 μm, Neomat Co. – Latvia,), Si (grade AX05 99.9% pure, FSSS 3.5 μm, H.C. Starck – Germany,) and B_4C (grade HS, FSSS 0.8 μm, H.C. Starck – Germany) were selected. In accordance with the following reaction

$$(2+x)\mathrm{Hf} + (1-x)\mathrm{Si} + \mathrm{B_4C} \Rightarrow 2\mathrm{HfB_2} + (1-x)\mathrm{SiC} + x\mathrm{HfC} \quad (1)$$

the correspondent stoichiometric precursors were weighed for $x = 0.2$. Such a formulation, adjusted by adding limited quantities of HfB_2 (99.5% pure, 325 mesh, Cerac Inc. – USA) and α-SiC (grade UF25, FSSS 0.45 μm, H.C. Starck – Germany), was milled for 24 h in a polyethylene jar using absolute ethanol and ZrO_2 balls, dried with a rotary evaporator under a continuous stream of nitrogen, and sieved. The expected final composition (vol%) reads $HfB_2 + 22.1$ SiC + 5.9 HfC.

In order to investigate the end-product formation kinetics of reaction (1), a rational campaign of (pressureless) heat treatments, hereafter labelled PLSHT-*n*, was conducted on the as-ground powder mix from 1000 °C up to 1650 °C in flowing Argon, with a heating rate of 10 °C/min and 1 h of dwell time, using graphite heating elements and crucibles (Astro Industries Inc. – USA). Compacted pellets (about 2 g in weight, 12 mm in diameter) were isostatically cold-pressed at 3500 kg cm^{-2}. After the heat treatments, the PLSHT-*n* pellets were finely crushed in an agate mortar, and then analyzed via X-ray diffraction (XRD, Ni-filtered Cu Kα radiation, mod. D500, Siemens – Germany). Thermodynamic calculations were performed using the HSC software package [12].

The reactive hot-pressing was performed at low vacuum (0.5 mbar) using a BN-lined induction-heated graphite die, into which the as-ground powder mix was directly loaded and heat-treated. The schedule of the thermal treatment is depicted in Fig. 1. The final set point of the hot-press run was 1900 °C. The temperature was measured with a pyrometer focused on the graphite die.

The bulk density was measured using the Archimedian method, while the relative density was estimated applying the rule of mixture. The microstructure was analyzed with a scanning electron microscope (SEM, Leica Cambridge, mod. S360, UK) equipped with an energy dispersive microanalyzer (EDX, mod. INCA Energy 300, Oxford Instruments Analytical, UK), and an X-ray diffractometer as well. Polished sections (finished 0.5 μm) of the reactive hot-pressed material were prepared using diamond abrasives.

Micro-hardness (Hv1.0) was measured by a Vickers indenter with 9.81 N as applied load for 15 s on a polished section. Flexural strength (σ) in a 4-pt. configuration was tested at two temperatures, 25 and 1500 °C, in ambient air on $25.0 \times 2.5 \times 2.0$ mm^3 chamfered bar (length × width × thickness, respectively), using 20 and 10 mm as outer and inner span, respectively, and a cross-head speed of 0.5 mm min^{-1}.

Likewise, two oxidation treatments (at ambient pressure)

(T-1) isothermal run at 1450 °C for 20 h in flowing dry air (50 cm^3 min^{-1}), 30 °C min^{-1} of heating rate and free cooling;
(T-2) isothermal cycled run at 1700 °C, 10 min of exposure each, loading and removal of the coupon at the fixed set-point

were carried out. Coupons with dimensions of $2.5 \times 2.0 \times 8.0$ mm^3 (surface finish $R_a \sim 0.2$ μm) were washed in an ultrasonic bath of acetone, and then dried

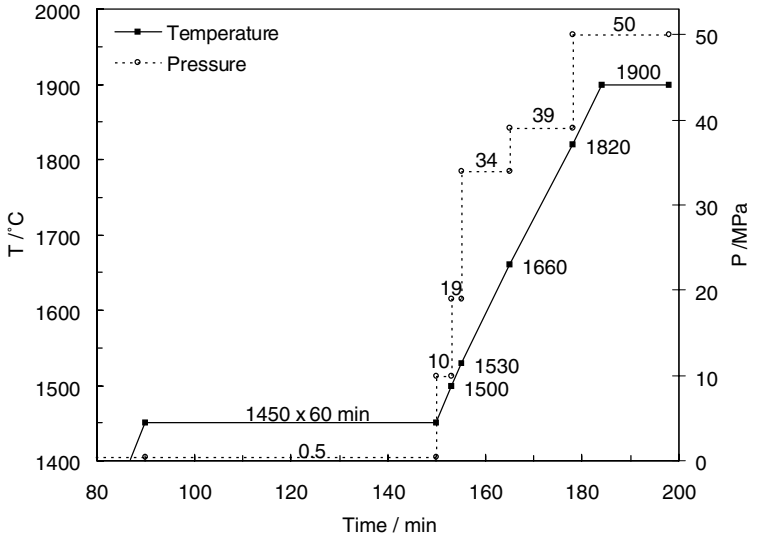

Fig. 1. Schedule of the reactive hot-pressing experiment: temperature (T, left Y-axis) and applied pressure (P, right Y-axis) vs. processing time. The temperature of 1450 °C was reached in about 90 min.

at 80 °C overnight. Treatment T-1 was executed using a thermogravimetric analyzer (mod. STA409, NETZSCH Gerätebau GmbH – Germany), 10^{-3} mg of accuracy, equipped with a vertically heated Al_2O_3 chamber. The test piece was placed upon zirconia supports, separating them from the Al_2O_3 holder. Treatment T-2 was performed using a bottom-loading box furnace, heated with $MoSi_2$ elements. The test specimen was placed upon SiC supports. The mass of the sample was measured before and after each cycle. Polished cross-sections of the oxidized samples were prepared and analyzed via SEM–EDX. The specimens (polished) surface, imaged using secondary electrons (SEs), were all observed free of conductive coating in order to maintain the sensitivity to the light elements of the EDX equipment as high as possible. In addition, using an optical microscope, the final thickness of the oxidized samples was measured as well.

3. Results

3.1. The ceramic synthesis via solid-state precursors

Processing parameters and some results from the series of the pressureless heat treatments (PLSHT-n) are shown in Table 1. Stacked XRD patterns from the starting as-ground mixture (PLSHT-0) and after treatments at 1000, 1100 and 1200 °C are presented (Fig. 2). In the mixture PLSHT-0, apart from α-Hf, Si and B_4C, X-ray diffraction identified also a cubic modified $HfH_{1.5}$ (ICDD 05-639) and HfB_2. The former was initially present in the as-received hafnium powder because of the wet storage. Such a hafnium hydride proved to be stable up to 1100 °C. Instead, the formation of HfB_2 during ball-milling clearly highlights how reaction (1) is prone to have succeeded (−695 kJ/mol enthalpy of

Table 1
Parameters and results of the PLSHT-n tests: temperature T, dwell time t, relative weight loss WL, and crystalline end-products

Test	T (°C)	t (min)	WL (%)	Crystalline end-products[b]	
				Main	Minor
PLSHT-1	1000	60	1.3	Hf[a], Si, HfB_2, HfC, $HfH_{1.5}$, B_4 C	(Hf,Si)
PLSHT-2	1100	60	1.5	Hf[a], (Hf,Si), HfB_2, HfC	–
PLSHT-3	1200	60	2.3	HfB_2, SiC, HfC	m-HfO_2
PLSHT-4	1300	60	1.0	HfB_2, SiC, HfC	m-HfO_2
PLSHT-5	1450	60	0.5	HfB_2, SiC, HfC	m-HfO_2
PLSHT-6	1500	60	1.0	HfB_2, SiC, HfC	m-HfO_2
PLSHT-7	1500	120	1.1	HfB_2, SiC, HfC	m-HfO_2
PLSHT-8	1550	60	1.4	HfB_2, SiC, HfC	m-HfO_2[c]
PLSHT-9	1600	60	1.2	HfB_2, SiC, HfC	–
PLSHT-10	1650	60	1.5	HfB_2, SiC, HfC	–

[a] Hexagonal type (ICDD 38-1478) but longer lattice parameters.
[b] Pulverized sample.
[c] Uncertain.

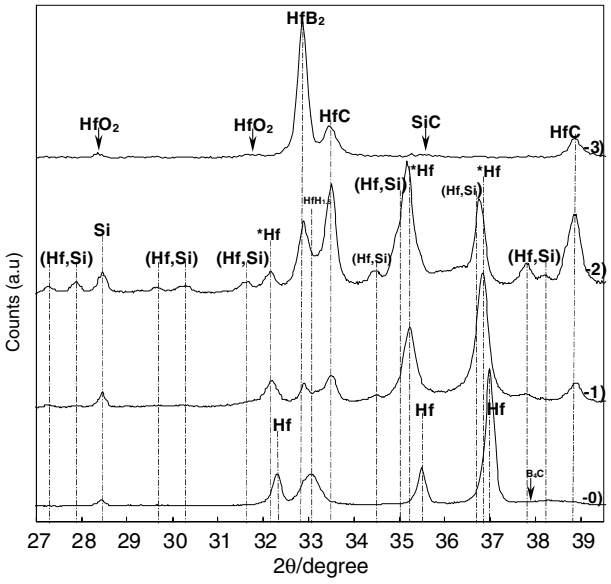

Fig. 2. XRD patterns of sample PLSHT-0 (as-ground), PLSHT-1 (1000 °C), PLSHT-2 (1100 °C) and PLSHT-3 (1200 °C). *Hf: ICDD 38-1478 but longer lattice parameters.

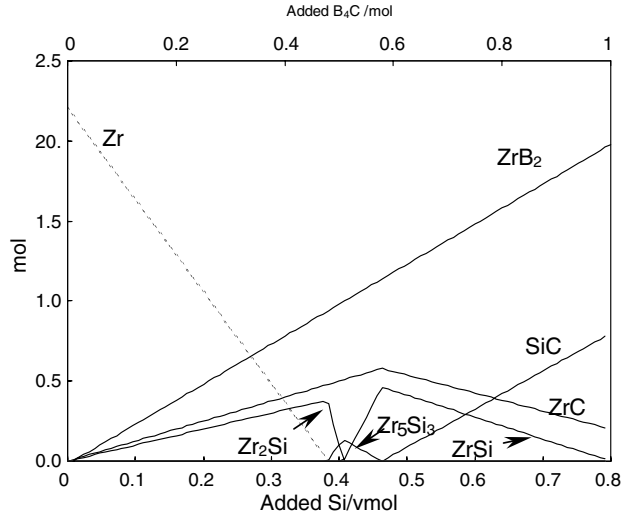

Fig. 3. Multiphase equilibrium composition calculated at 25 °C, and 2.2 mol Zr as starting amount. Silicon and boron carbide are progressively added up to 0.8 and 1 mol, respectively.

formation at 25 °C), and satisfies also the thermodynamic conditions for a self-sustaining reaction process ($T_{ADIAB} \cong 2900$ °C).

In accordance with the XRD outcomes (Fig. 2), reaction (1) proceeded to a certain extent at 1000 °C, until the consumption of the initial precursors was completed at 1200 °C and 1 h of dwell time. Within the temperature range 1000–1200 °C, several chemical reactions take place, giving rise to stable intermediate solid by-products. In particular, the emergence of a mixture of hafnium silicides, most probably Hf_5Si_4 and Hf_5Si_3, was ascertained. In contrast to other IVB group transition metals like titanium and zirconium, reliable thermochemical data for the family of hafnium silicides are unavailable. However, having assumed highly plausible the chemical affinity of Hf with respect to Zr, and hence of the present studied system with an Zr–Si–B_4C one, a multiphase equilibrium composition was calculated as well (Fig. 3). Such an exercise basically intended discerning the predominance of the chemical reactions evolving during the studied synthesis. The conversion rates do not change appreciably by increasing temperature. Thus, from a thermodynamic point of view, it can be argued that reaction (1) proceeds independently of the set temperature. A specific discussion will be presented later.

Raising the processing temperature of the PLSHT-*n* test up to 1650 °C, the end-products of the synthesis vary slightly in composition and relative percentages. The XRD pattern of sample PLSHT-5 is shown in Fig. 4.

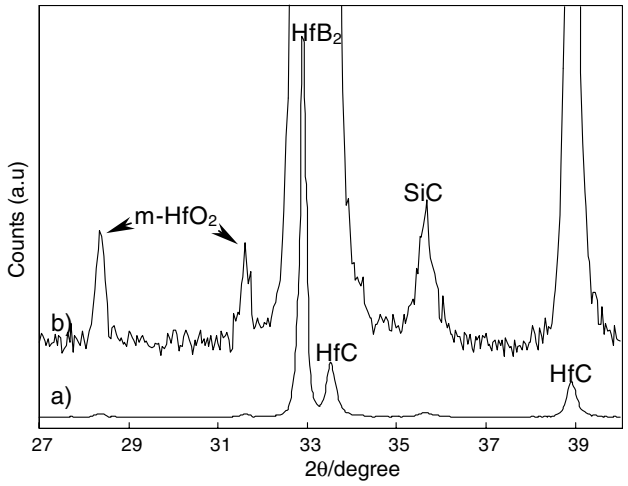

Fig. 4. XRD pattern from sample PLSHT-5 (1450 °C for 1 h): normal view (a), expanded full scale (b).

3.2. The reactive hot-pressed composite

3.2.1. Microstructure

The processing conditions of the PLSHT-5 treatment were adopted for the ceramic synthesis during the reactive hot-pressing. In fact, the as-ground powder mixture was loaded straight into the hot-press equipment and heat-treated, in accordance with the thermal programme shown in Fig. 1. The heating rate from about 900 up to 1450 °C was kept as low as 10 °C min^{-1} in order to quench any emergence of spontaneous self-combustion, whilst the external pressure was stepwise applied only once the synthesis at 1450 °C for 60 h had finished.

The terminal stage was 1900 °C for 10 min, 50 MPa of applied pressure.

In accordance with the full completion of reaction (1), the predicted bulk density of the composite is 9.51 g cm^{-3}. The measured bulk density was 9.43 g cm^{-3}, 0.992 of the theoretical relative density. The XRD analysis of the hot-pressed composite (Fig. 5) established the formation of HfB_2, SiC, HfC, *m*-HfO_2 as secondary phase, and a slight 001 texture of the diboride matrix. The estimated amounts (vol%) of the mentioned phases (Fig. 5) agree with those predicted on the full completion of reaction (1) (72 HfB_2, 22.1 SiC, 5.9 HfC). It follows that all the silicon introduced in the starting mixture reacts with the available carbon (from B_4C) and yields the expected amount of SiC. The lattice parameter of the cubic hafnium carbide, 0.46230 ± 0.0005 nm, slightly departs from the reference value of 0.463765 nm (ICDD 39-1491). Thus, the occurrence of a non-stoichiometric HfC is highly plausible.

The composite bulk, inspected by SEM, does not reveal residual porosity. A final relative density of 0.992 congruently agrees with a microstructure free of porosity. The general configuration of the microstructure (Fig. 6(a)) presents regularly faceted diboride grains (from 0.5 to 4 μm as grain size) and intergranular SiC particulates (about 2 μm max as grain size). Considering the relatively high temperature applied, the grain size remains rather fine. The fracture mode is chiefly intergranular even if, in correspondence with the largest grains, intragranular events seem to prevail. Microcracking of HfB_2 grains and debonding of SiC/HfB_2 interfaces are observed. The emergence of tensile or compressive residual strained fields in the diboride matrix and SiC particulates, respectively, was considered the main reason of such a phenomenon. Further SEM–EDX examinations of polished regions identified the main solid constituents (Fig. 6(b)). The grain size of SiC varies within few micrometers. The diboride/diboride interfaces seem depleted of secondary phases.

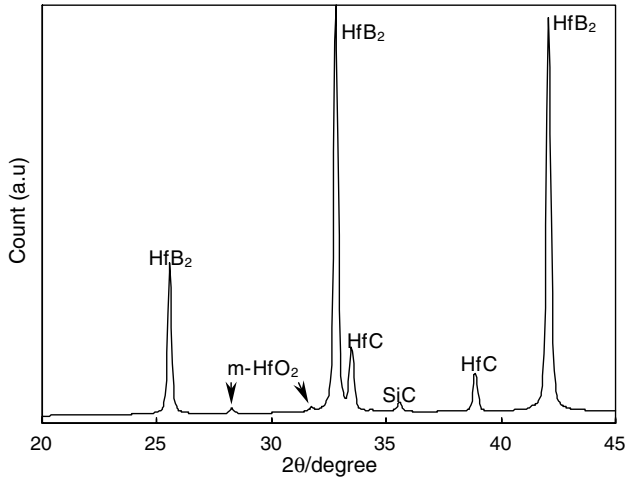

Fig. 5. XRD pattern of the reactive hot-pressed composite: the volumetric amounts of HfB_2 (71%), SiC (21%), HfC (7%), and HfO_2 (1%) were estimated, using a Rietveld routine. The 001 crystallographic orientation of the HfB_2 matrix is evident.

Differently from previous studies on HfB_2–SiC systems including small quantity of additives [13,14], the reaction products associable to a residual liquid phase were not found. This corroborates the concern that solid-state diffusion drove the transfer of matter during sintering, and that undesired thermally unstable secondary phases were most likely suppressed.

3.2.2. Mechanical properties

The experimental values of some mechanical properties are summarized in Table 2. In terms of absolute value, the Young's modulus (*E*) agrees with that reported

Table 2
Mechanical properties of the reactive hot-pressed composite: Young's modulus *E*, micro-hardness Hv1.0, 4-pt. flexural strength σ at 25 and 1500 °C

E (GPa)[a]	Hv1.0 (GPa)[b]	σ (MPa)[b]	
		25 °C	1500 °C
520 ± 4	19.0 ± 1.0	770 ± 35	310 ± 15

[a] Uncertainty.
[b] (mean ± 1 SD).

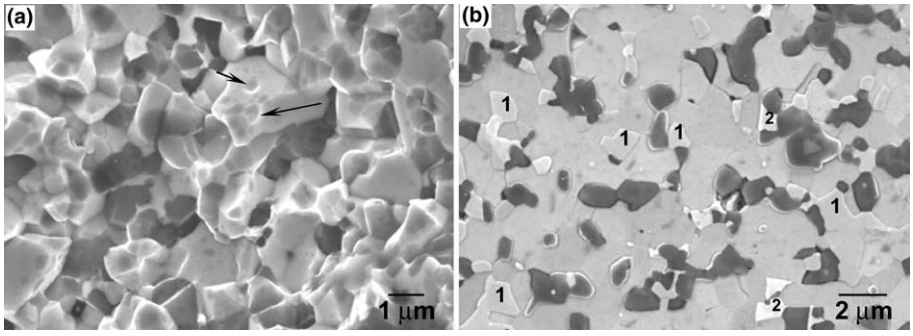

Fig. 6. SEs-SEM micrographs from a fracture (a) and a polished surface (b) of the reactive hot-pressed composite. (a) The arrows mark the imprinting of SiC particles upon HfB_2 grains. (b) Some grains of HfC (1) and HfO_2 (2) are indicated; darker micrometric features consist of intergranular SiC particles.

for a similar fully dense HfB_2–20 vol% SiC ceramic [3]. The flexural strength at room temperature exhibits a really impressive mean modulus of rupture for this category of UHTCs. Likewise, the narrow dispersion of data points out the suitability of the processing procedures which enable some control over manufacture flaws. At 1500 °C, a reduction in strength occurred. The load–displacement curve deviates to some extent from linearity (Fig. 7). The micro-hardness (Hv1.0) is rather high: the presence of hard ingredients like HfB_2 and SiC is not adversely affected either by residual porosity or by a coarse microstructure.

3.2.3. The resistance to oxidation

The mass change (w) vs. temperature (T) or vs. exposure time (t) during the treatment T-1 is shown in Fig. 8. The pattern of the thermogravimetric (TG) curve along the heating stage (Fig. 8(a)) is closely connected to the thermal instability of the oxide scale growing upon the external faces of the oxidizing sample. The temporary stationary branch between 1280 and 1400 °C of the TG data basically results from a balance between the release of gaseous by-products like B_2O_3 and CO, and the transformation of HfB_2 and HfC into HfO_2. An offset of 0.35 mg cm^{-2}, which accounts for the oxidation preceding the planned exposure, was subtracted from the TG data over the isothermal stage (Fig. 8(b)). Applying the model proposed by Nickel [15], the multiple linear-regression of the paralinear law $w = K_{PAR}\sqrt{t} + K_{LIN}t$ (K_{PAR} and K_{LIN} constants) fits the TG data very well. This calculation points out that the oxidation process is rate-limited by diffusional mechanisms. The XRD analysis of the exposed surfaces detected monoclinic HfO_2, highly textured $HfSiO_4$, and SiO_2 cristobalite in minor content. The SEM–EDX inspection of the cross-section (Fig. 9(a)) highlights an external scale, basically consisting of a silica glass (Fig. 9(b)). Local ruptures of the external oxide scale were not observed. The undulating thickness of such a glassy coating indicates that, owing to a diminished viscosity at the testing temperature, it may laterally flow out. Underneath this glassy layer, an oxide scale extending up to the as-sintered virgin bulk is basically constituted of $HfSiO_4$ and monoclinic HfO_2. Both these oxides crystals are enclosed by a glassy melt, the former lying along the bottom of the outermost silica glass.

As far as the oxidation treatment T-2 is concerned, the mass gain (mg cm^{-2}) were 1.60 ± 0.05 and 1.85 ± 0.05 after 10 and $10 + 10$ min of exposure, respectively. The scheme of the microstructural alteration (Fig. 10) differs a little from that just described (Fig. 9(a)). Apart from the external glass, only HfO_2 crystals embedded in the glassy melt compose the underlying scale. Underneath this oxide scale, an additional

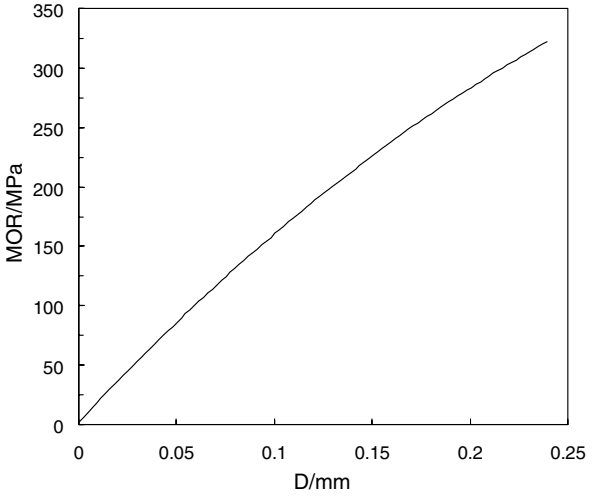

Fig. 7. Load (MOR) vs. displacement (D) curve, recorded at 1500 °C during 4-pt flexural strength test.

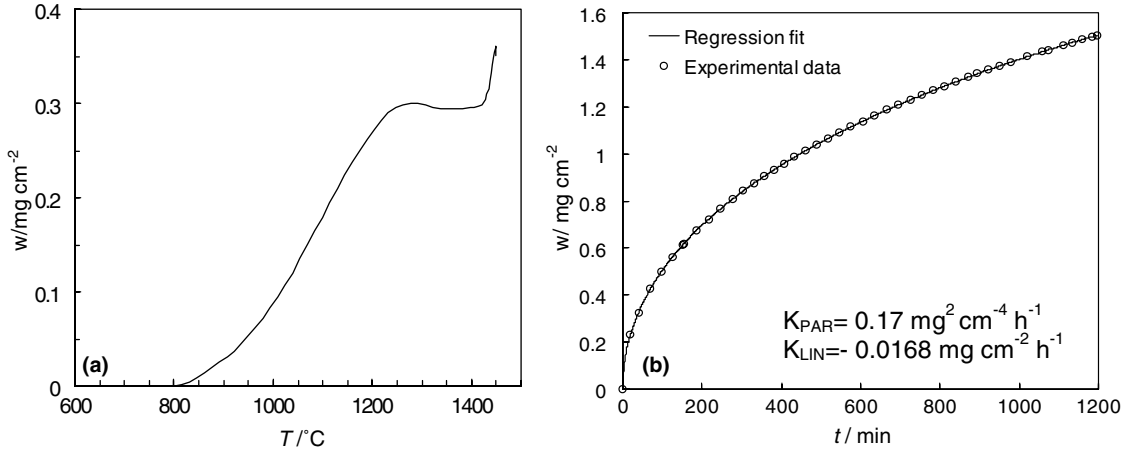

Fig. 8. Thermogravimetric data of the treatment T-1: weight change w vs. temperature T (a) or vs. exposure time t (b). The best fitted parameters K_{PAR} and K_{LIN} are shown.

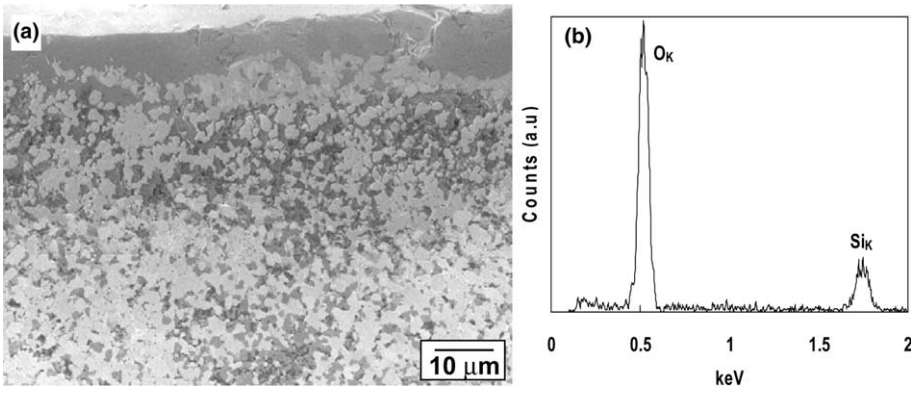

Fig. 9. SEs-SEM micrograph from a polished cross-section of the hot pressed composite, after oxidation at 1450 °C for 20 h (a), and EDX spectrum ((b) 4 keV electron beam energy) of the external glass (upper part of the micrograph).

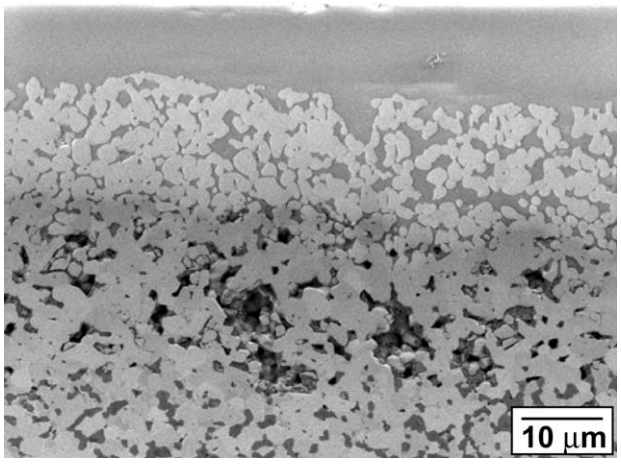

Fig. 10. SEs-SEM micrograph from a polished cross-section of the hot pressed composite, after oxidation at 1700 °C for 2×10 min. The upper part of the micrograph is occupied by a silica based glassy coating.

porous band has formed in consequence of the active oxidation of the SiC particulates herein located. After $10 + 10$ min of exposure, the thickness of the oxidized specimen had an increase of about 20 μm.

4. Discussion

4.1. The "in situ" synthesis of the HfB_2–SiC–HfC mixture

The "in situ" synthesis of the HfB_2–SiC mixture proceeded via decomposition and further mass exchange processes at high temperatures. Of course the solid precursors (i.e., Hf, Si and B_4C) were selected such that the resulting reaction was highly exothermic. The real driving force of such solid-state exchange reactions definitely arises from the formation of thermodynamically very stable end-products.

The strong exothermicity of the studied system of reactants switched a sort of mechanically induced formation of by-products during ball-milling. In particular, apart from a predictable reduction in size of the ball-milled powders, an accumulation of defects in the powder particles introduces additional energy to the reactant system in the form of interfacial and strain energies. Such extra available energy leads part of the intimately mixed components to chemically react in this way, $2Hf + B_4C = 2HfB_2 + C$, without the help of external thermal inputs. The formation of an inert compound like HfB_2 plausibly quenches other reactions from self-propagating during mechanical mixing. Likewise, an heating rate of 10 °C min^{-1} during PLSHT tests smooths any occurrence of spontaneous combustion.

The multi-component equilibrium composition (Fig. 3) along with the support of XRD analyses on the PLSHT samples, helped in tracing a sequence of some transitory steps of reaction (1). By analogy with a similar system [16], the following chemical reactions (dG_{25}: Gibbs free energy of reaction at 25 °C)

$$2Hf + B_4C = HfB_2 + HfC \ (dG_{25} = -794 \text{ kJ/mol}) \quad (2)$$

$$xHf + ySi = Hf_xSi_y, \quad x/y = 5/4, 5/3 \quad (3)$$

$$2HfC + 3Si + B_4C = 2HfB_2 + 3SiC \ (dG_{25} = -386 \text{ kJ/mol}) \quad (4)$$

$$HfC + Hf_5Si_4 + 3B_4C = 6HfB_2 + 4SiC \quad (5)$$

are guessed to occur. A lack of thermochemical data for the Hf–Si system does not permit the dG values of reaction (3) and (5) to be calculated, even if, similarly to Zr–Si or Ti–Si systems, large negative dG values are expected. Likewise, the predominance of specific hafnium silicides at different temperatures logically depends on the activity ratio a_{Hf}/a_{Si} of the available metallic Hf and Si. Also, reaction (4) and (5) describe the delayed formation of SiC, only once an appreciable amount of HfC has already formed. The XRD pattern of sample

PLSHT-2 show robust peak intensities belonging to HfC and some hafnium silicides (Fig. 2). Increasing temperature up to 1200 °C, reaction (4) and (5) become prevailing, giving rise to the desired formation of HfB_2 and SiC.

This representation intended to highlight the dominant chemical reactions. The finite size of the powdered precursors, for instance, often put in contact only some of them, favouring reactions which may yield minority products. The XRD patterns of sample PLSHT-2 and PLSHT-3 still contain minor unindexed peaks. The application of synthesis temperatures from 1300 up to 1650 °C does not imply significant changes in the stoichiometry of the end-products (Table 1). Nevertheless, the reduction of the peak width reflects the predictable increase in size of HfB_2, SiC and HfC crystallites. Moreover, the gradual disappearance of the HfO_2 phase is explained by its conversion into HfC. The carbon-rich reducing environment favours the transformation of HfO_2 into HfC, according to the following reaction

$$HfO_2 + 3C = HfC + 2CO(g) \quad (6)$$

which has negative dG above 1375 °C. Finally, for temperatures above 1600 °C, the conversion yield of HfC starts dominating over that of SiC. Therefore, 1450 °C was deemed an acceptable temperature for synthesizing as fine as possible solid constituents for the final composite and, at the same time, for promoting the formation of HfB_2 and SiC against the competing raise of HfC.

4.2. Reactive hot-pressing, microstructure and mechanical properties

Compared to the hot-pressing conditions of an additive-free HfB_2–20 vol% SiC powder mixture (2200 °C for 1 h and 25 MPa [3]), the present material experienced a less intensive thermal history. This represents a very important issue because the intrinsic poor sinterability of a mechanically mixed HfB_2–SiC powder system is overturned by a correct selection either of the precursors and of the heat treatments.

The initial fineness of the powder mixture is decisive in obtaining well dispersed and fine-grained solid phases constituting the sintered composite. Once B_4C decomposes, boron and carbon readily diffuse and interact with the metallic precursors Hf and Si. This feature is supported by the evidence that the "in situ" synthesized solid HfB_2 and SiC keep the dimensional ranges of the starting precursors.

The densification rate of diboride powders is known being greatly influenced by the boron activity. A contamination in oxygen, typically present upon the diboride particle surfaces, entails a decrease in the boron activity (i.e., reduction of the densification rate), and brings on grain-coarsening at the processing temperature required for achieving near full density [17,18]. Differently from HfB_2 powders usually stored and manipulated in air before hot-pressing [3,5,13,14], in the present study the surfaces of the HfB_2 particulates ("in situ" synthesized in a inert atmosphere) are supposed being only slightly affected by the oxygen contamination. Further conditions of an intimate contact between oxygen-depleted reacting interfaces of diborides and the contemporary application of high temperature and pressure most likely facilitate surface/boundary diffusion, and assist densification, the boron activity being no further depressed.

In addition, similarly to an analogous ZrB_2–SiC system [19], the acceleration in densification is compensated by the dragging action of SiC, which, by virtue of its own refractoriness, limits extensive growth of the HfB_2 matrix. Some grooves imprinted all around the HfB_2 grains may be convincing evidence of the role of SiC in controlling growth of the diboride matrix (Fig. 6). Despite a sintering temperature of 1900 °C, the final average grain size of the tested material does not exceed a few micrometers.

Clean diboride/diboride or diboride/carbide boundaries, already reported for an "in situ" synthesized TiB_2–SiC system [16], support the supposition of tight interfacial joinings. Such a merit can be ascribed to the high surface energy of the newly formed diboride grains, and indicates that the tightening SiC particles formed in situ strongly connect with the diboride matrix. This inference should be validated by assessing at nanometric level the absence of foreign phases along grain boundaries, that analyses (herein presented) verified only with the SEM–EDX technique.

As far as the mechanical characterization is concerned, a Young's modulus of 520 GPa is in very good agreement with that calculated (i.e., 505 GPa) using a rule of mixture [20], namely the arithmetic average $\Sigma Q_i E_i$, Q_i the volume fractions of phases constituting the composite. For E_i and Q_i the following data were used: 530 GPa [21] and 0.71 for HfB_2, 460 GPa [22] and 0.06 for HfC, 448 GPa [23] and 0.22 for SiC, and 239 GPa [21] and 0.01 for HfO_2. Control of the residual porosity along with of the secondary phases characterized by low E values (i.e., HfO_2) is of fundamental importance against the depression of this property.

In the results section, the opening of HfB_2/SiC interfaces and some microcracking of HfB_2 grains were reported occurring after cooling. A representative example is shown in Fig. 11. The extent of the residual thermal stresses which involve the HfB_2/SiC interfaces was calculated in accordance with the formula proposed by Eshelby [24]. It basically considers spherical particles embedded in an infinite matrix (in our case SiC and HfB_2, respectively) but does not take into account the volume fractions of the phases constituting the composite. Actually, as far as the HfB_2–SiC system is

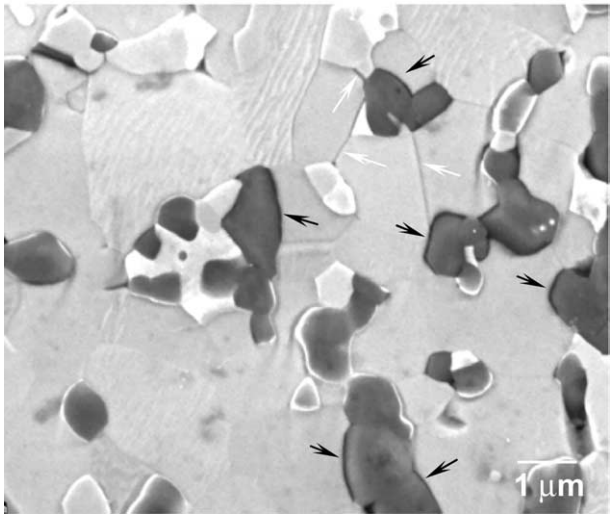

Fig. 11. SEs-SEM micrograph from a polished section of the as-sintered composite: black and white arrows mark examples of disjoined HfB_2/SiC interfaces and microcracked HfB_2 grains, respectively.

concerned, referenced assignments of the freezing temperature value T_{FR}, which commonly indicates the temperature range along the cooling stage within which the stresses are not released by atomic diffusion, are not available. Differently from other authors which set T_{FR} equal to 1200 °C [6], the strong refractoriness of an HfB_2–SiC system is plausible to call for the input of larger T_{FR} value around 1800 °C. Magley et al. [25] utilized a T_{FR} value of 1700 °C for a SiC–TiB_2 particulate composite. Another proposal modelled by Mizutani on a SiC-rich ZrB_2 composite extrapolated a value of T_{FR} equal to 1750 °C [26]. On substitution of the appropriate values, tensile stressed HfB_2 and compressive stressed SiC are expected (Table 3). Therefore, the microcracking events are attributed to the emergence of high residual stresses which come up at the HfB_2/SiC interfaces in consequence of the mismatch of structural properties like E, thermal expansion (λ) and Poisson's ratio (v). Such a first approximation, based on the HfB_2 matrix – SiC particle model, overlooks the presence of HfC. On the other hand, only HfB_2 and SiC were involved in these localized micro-mechanical phenomena. In addition, the input of the following values ($T_{FR} = 1800$ °C, $E = 460$ GPa, $v = 0.18$, $\lambda = 6.5 \times 10^{-6}/°C^{-1}$ [22]) in the Eshelby formula foresees compressive radial stresses for HfC (−1.095 GPa) and tensile stresses (0.55 GPa) for HfB_2. It follows that, in the economy of this basic estimate, the presence of 6 v/o HfC can realistically be overlooked.

Table 3
Estimation of the residual stresses (σ_{RES}) at the matrix/particle interface (E, Young's modulus; λ, linear thermal expansion coefficient; v, Poisson's ratio)

	E (GPa)	λ 10^{-6} (°C)	v	σ_{RES} (GPa)
HfB_2 (matrix)	530	8	0.12 [21]	1.407
SiC (particle)	448	4	0.168 [23]	−2.815

The flexural strength and relative dispersion (Table 2) exhibit excellent values, at room temperature and 1500 °C. At 1500 °C, the refractoriness of HfB_2 and SiC, which compose the composite skeleton, ensures the strength is retained efficiently. Without any plastic deformation of the test bar taking place, the slight downward curvature of the load–displacement curve (Fig. 7) is connected to the sub-critical crack growth. SEM observations of the surfaces fractured at 1500 °C confirmed the occurrence of this phenomenon. Actually, the microstructural degradation on the specimen tested at 1500 °C adversely contributes to the decrease in strength. Most of the HfC grains directly facing the oxidizing atmosphere for instance react readily, transforming into an oxide form. However, the inner parts of the specimen are protected from further attack by the ability of the outermost oxidation product like a silica-based glass to seal the external surfaces, thus preventing the strength being further impaired.

The initial compositional design of the composite aimed at introducing a moderate level of HfC in a HfB_2 + SiC skeleton. This specific feature was reported to have succeeded in improving oxidation/ablation resistance of diboride–SiC materials subjected to heating regimes simulating hypersonic re-entry space missions [27]. However, with reference to the strength behaviour in air up to 1500 °C (conditions that differ markedly from those just mentioned), increasing the content of HfC negatively affects the ability of HfB_2–SiC composites to retain the original strength effectively.

4.3. The resistance to oxidation

The present study highlighted how limited mass gains are accompanied by a few alterations of the original microstructure. In agreement with other authors [10,11,27,28], the presence of SiC particles substantially enhances the resistance to oxidation of a pure HfB_2. It's known that the oxidation of HfB_2 and HfC generates HfO_2 and amorphous B_2O_3, or HfO_2 and CO(g), respectively. The increase in the scaling rate above 800 °C (Fig. 8) is primarily caused by the selective oxidation either of the HfB_2 and HfC, with no appreciable attack of the SiC particles. The external oxide scale that forms partially allows the diffusion of oxygen through interconnected pores or via lattice vacancies in HfO_2. Similarly to ZrO_2, HfO_2 behaves plausibly as an anionic conductor. In addition, at a relatively high temperature, a fluid B_2O_3 (melting point of 450 °C), which most likely covers the external faces of the oxidizing sample, is known to be much more permeable to oxygen than a silica glass [29]. The almost stationary trend of the TG data

between 1280 and 1400 °C (Fig. 8) accounts for the balanced competition between mass losses and gains.

Substantial benefits from the presence of the SiC particles result for temperatures above 1400 °C. In accordance with the following reaction, $SiC + 3/2\ O_2(g) = SiO_2 + CO(g)$, silica which forms from the oxidized SiC particles combines with the available boria, providing more oxidation protection than the HfO_2 alone. Likewise other MB_2–SiC systems, M = Zr or Hf [10,11,28,30,31], the exposed faces of the present composite are covered by an adherent silica-based glass (Fig. 9(b)), which in turn is characterized by an undulating thickness. This glass, scarcely permeable to oxygen at the tested temperature [29], seals and protects the external surfaces of the sample. The evidence of residual unoxidized SiC particles just beneath the external oxide scale settles the fundamental role of such a phase in slowing the advance of the oxidation attack (Fig. 12).

TG data of the isothermal test T-1 fit a paralinear law very well (Fig. 4). The parabolic contribution dominates the monotonically decelerating trend of the TG data. In effect, the growth of a protective external oxide scale progressively imposes longer diffusion paths for oxygen to arrive at the diboride–oxide interface. The departure from a pure parabolic pattern is described by a little negative linear contribution, and is most likely motivated by a release of some gaseous oxidation by-products like CO(g) and B_2O_3(g). Moreover, the apparent cleanness of the diboride–diboride boundaries (i.e., absence of intergranular compounds) has a beneficial merit in limiting the preferential inward transport of oxygen through them (Fig. 12).

As far as the treatment T2 is concerned, the intrinsic refractoriness of the studied system and the protection of the external glassy coating supply the thermostructural stability that enables the composite to withstand efficiently such severe thermal loads. In addition, the increase of about 20 μm in thickness of the oxidized sample after 10 + 10 min of exposure verifies that surface conversion and removal of mass have no appreciable effects.

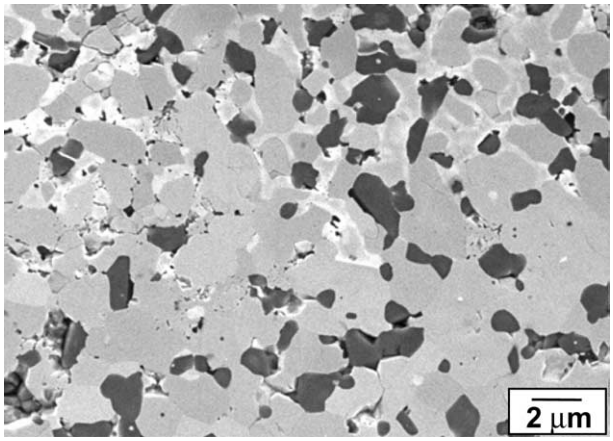

Fig. 12. SEs-SEM micrograph from a polished section of the oxidized sample (1450 °C for 20 h). Un-oxidized SiC particulates and oxidation advancing through the diboride grain boundaries are evident.

5. Summary

This work highlighted promising advances in the "in situ" synthesis, microstructure and mechanical properties of an ultra-high-temperature HfB_2–SiC composite. Solid powder precursors like Hf, Si and B_4C were properly processed via reactive hot-pressing, and a full dense HfB_2–SiC composite thus obtained. The full conversion of the starting reagents into the end-products (HfB_2, SiC, HfC) was "in situ" conducted during the reactive hot-press run at 1450 °C for 60 min. The final microstructure, mean grain size 3 μm, was uniform and rather fine, with HfO_2 as the principal secondary phase. The SiC phase basically played the role of inhibitor against excessive coarsening of the HfB_2 matrix. The flexural strength values were very promising: 770 ± 35 and 310 ± 15 MPa at 25 and 1500 °C, respectively. The Young's modulus was 520 GPa. The composite showed a rather good resistance to oxidation: repeated exposures at 1700 °C in air did not severely affect the overall integrity of the composite. This unconventional approach of "in situ" synthesizing/densifying strongly covalent ceramic–matrix composites was an novel answer to fabricating ultra-refractory materials.

Acknowledgements

I sincerely acknowledge the helpful contribution of the colleagues D. Dalle Fabbriche (thermal treatments), C. Melandri (mechanical tests), and A. Balbo (oxidation tests).

References

[1] Upadhya K, Yang J-M, Hoffman WP. Materials for ultra-high temperatures structural applications. Am Ceram Soc Bull 1997;58:51–6.
[2] Wang CR, Yang J-M, Hoffman WP. Thermal stability of refractory carbide/boride composites. Mater Chem Phys 2002;74:272–81.
[3] Gasch M, Ellerby D, Irby E, Beckman S, Gusman M, Johnson S. Processing, properties and arc-jet oxidation of hafnium diboride/silicon carbide ultra high temperature ceramics. J Mat Sci 2004;39:5925–37.
[4] Opeka MM, Talmy IG, Wuchina EJ, Zaykoski JA, Causey SJ. Mechanical, thermal and oxidation properties of refractory hafnium and zirconium compounds. J Eur Ceram Soc 1999;19:2405–14.
[5] Bull J, White MJ, Kaufman L. Ablation resistant zirconium and hafnium ceramics. US Patent 5,750,450, 1998.

[6] Zhang GJ, Deng ZY, Kondo N, Yang JF, Ohji T. Reactive hot pressing of ZrB_2–SiC composites. J Am Ceram Soc 2000;83(9):2330–2.
[7] Zhang GJ, Ando M, Yang JF, Ohij T, Kanzaki S. Boron carbide and nitride reactants for in situ synthesis of boride-containing ceramic composites. J Eur Ceram Soc 2004;24:171–8.
[8] Blum YD, Kleebe H. Chemical reactivities of hafnium and its derived boride, carbide and nitride compounds at relatively mild temperature. J Mat Sci 2004;39:6023–42.
[9] Gillan EG, Kaner RB. Synthesis of refractory ceramics via rapid metathesis reactions between solid-state precursors. Chem Mater 1996;8:333–43.
[10] Opeka MM, Talmy IG, Zaykoski JA. Oxidation-based materials selection for 2000 °C + hypersonic aerosurfaces: theoretical considerations and historical experience. J Mat Sci 2004;39:5887–904.
[11] Opila E, Levine S, Lorincz J. Oxidation of ZrB_2- and HfB_2-based ultra-high-temperature ceramics: effect of Ta additions. J Mat Sci 2004;39:5969–77.
[12] HSC chemistry for windows 5.11, Outokumpu Research Oy, Pori Finland.
[13] Monteverde F, Bellosi A. Microstructure and properties of an HfB_2–SiC composite for ultra high temperature applications. Adv Eng Mater 2004;6(5):331–6.
[14] Monteverde F, Bellosi A. The efficacy of HfN as sintering aid in the manufacture of ultra-high temperature diboride HfB_2 matrix ceramics. J Mater Res 2004;19(12):3576–85.
[15] Nickel KG. Multiple law modelling for the oxidation of advanced ceramics and a model-independent figure of merit. In: Nickel KG, editor. Corrosion of advanced ceramics/measurements and modelling. Dordrecht: Kluwer Academic Publishers; 1994. p. 59–71.
[16] Zhang GJ, Yue XM, Jin ZZ, Dai JY. In-situ synthesized TiB_2 toughened. SiC J Eur Ceram Soc 1996;16:409–12.
[17] Ovrebo DN, Riley FL. Densification of zirconium diboride. In: Conference and exhibition of 6th EcerS, extended abstract vol. 2, British Ceramic Proceedings No. 60, London: IOM Communication Ltd.; 1999. p. 19–20.
[18] Baik S, Becher PF. Effect of oxygen contamination on densification of TiB_2. J Am Ceram Soc 1987;70:527–30.
[19] Monteverde F, Guicciardi S, Bellosi A. Advances in microstructure and properties of zirconium diboride based ceramics. Mat Sci Eng A 2003;346/1–2:310–9.
[20] Torquato S. Modelling of physical properties of composites materials. Int J Solids Struct 2000;37:411–22.
[21] Kotelnikov RB, Bashlykov SN, Galiakbarov ZG, Kashtanov AI. Handbook of high melting point materials. Moscow: Metallgiya Press; 1969.
[22] Brown HL, Armstrong PE, Kempter CP. Elastic properties of some polycrystalline transition-metal monocarbides. J Chem Phys 1966;45(2):547–9.
[23] MCIC Report HB-07-vol. 2 (Reprinted in July 1987). Engineering property data on selected ceramics, carbides. Metals and Ceramics Information Center, Battelle, Columbus OH.
[24] Eshelby JD. The elastic field outside an ellipsoidal inclusion. Proc R Soc London, A 1959;252:561–9.
[25] Magley DJ, Winholtz RA, Faber KT. Residual stresses in a two-phase microcracking ceramic. J Am Ceram Soc 1990;73(6):1641–4.
[26] Mizutani T. Residual strain energy in composites containing particles. J Mater Res 1996;11(2):483–94.
[27] Metcalfe AG, Elsner DT, Allen DT, Wuchina E, Opeka M, Opila E. Oxidation of hafnium diboride. High temperature corrosion and materials chemistry: per kofstad memorial symposium, electrochemical society proceedings, vols. 99–38. p. 489–501.
[28] Hinze JW, Tripp WC, Graham HC. The high-temperature oxidation behaviour of a HfB_2 + 20 v/o SiC composite. J Electrochem Soc 1975;122(9):1249–54.
[29] Doremus RH. Glass science. New York: Wiley; 1973. p. 138.
[30] Monteverde F, Bellosi A. The resistance to oxidation of an HfB_2–SiC composite. J Eur Ceram Soc 2004;25/7:1025–31.
[31] Levine SR, Opila EJ, Halbig MC, Kiser JD, Singh M, Salem JA. Evaluation of ultra high temperature ceramics for aeropropulsion use. J Eur Ceram Soc 2002;22:2757–67.